

# Diffusiophoresis and medium structure control macroscopic particle transport in porous media

Mamta Jotkar\*

*Universidad Politécnica de Madrid, Spain,  
Institute of Environmental Assessment and Water Research,  
Spanish National Research Council, Barcelona, Spain*

Pietro de Anna†

*Institute of Earth Sciences, University of Lausanne, Switzerland*

Marco Dentz‡

*Institute of Environmental Assessment and Water Research,  
Spanish National Research Council, Barcelona, Spain*

Luis Cueto-Felgueroso§

*Universidad Politécnica de Madrid, Spain*

(Dated: March 16, 2023)

In this letter, we show that pore-scale diffusiophoresis of colloidal particles along local salt gradients manifests in the macroscopic dispersion of particles in a porous medium. Despite its transient character, this microscopic phenomenon controls large-scale particle transport by altering their partitioning between transmitting and dead-end pores. It determines the distribution of residence and arrival times in the medium. Depending on the diffusiophoretic mobility, particles can be mobilized from or trapped in dead-end pores, which provides a means for the controlled manipulation of particles in porous media.

Keywords: Diffusiophoresis, anomalous dispersion, porous media

Diffusiophoresis (DP) [1] is the motion of microscopic particles driven by local gradients of solute concentration that has been demonstrated both theoretically [2–5] and experimentally [6–11] to be a powerful particle manipulation tool. The physical mechanisms that drive this complex physicochemical phenomenon can be broken down to two components: chemiphoresis that occurs due to the osmotic pressure gradient along the surface of a charged particle (at the scale of the particle) and electrophoresis arising due to the difference in the diffusivities between the cation and the anion in the electrolyte solution [4]. The physics behind this phenomenon is well-established [2, 3]. Despite the studies in relatively simpler microfluidic setups that demonstrate particle focusing [12], particle separation [13–16], particle banding [17], particle trapping [11], etc., with the help of DP, its effect on macroscopic transport within intricate and spatially variable porous structures remains unexplored.

Flow and transport of dissolved solutes and suspended particles through porous and confined media are ubiquitous in natural and engineered systems [18]. Most geological and biological porous media share the common feature of being spatially variable or heterogeneous. The broad range of variability in pore size is known to induce anomalous transport. Moreover, the diversity in

shape of the constituent grains induces a rich flow organization that plays an important role in groundwater contamination and remediation [19], enhanced hydrocarbon recovery [20], transport through river sediments [21] and water filtration systems [13, 22]. The morphology of a porous medium is often characterized by the presence of cavities or dead-end pores (DEP), which represent the part of the system that cannot host net fluid transfer, resulting in stagnant flow [23–25]. These DEPs are connected via a network of percolating channels or transmitting pores (TP). Such DEP-TP structures characterize biological tissues [26], soil [25] and filters [27] and lead to anomalous transport of passive tracers [28]. To date, the combined role of DP and the complexity of the porous medium on particle transport remains elusive. Here, we use detailed numerical pore-scale simulations and analytical modeling to elucidate how DP couples with the medium structure to alter macroscopic particles transport.

We study a fluid-saturated porous system where a particle suspension gets displaced by a continuously injected salt solution. The velocity experienced by each transported particle results from advection in the flow field  $\mathbf{u}$ , which is controlled by the medium structure and imposed flow rate [29–31], and due to the diffusiophoretic drift  $\mathbf{u}_{dp}$ . In the thin Debye layer limit, for dilute solutions with valence symmetric solutes (e.g., LiCl, NaCl), the diffusiophoretic drift is proportional to the gradient of the logarithm of the solute concentration

$$\mathbf{u}_{dp} = \Gamma_p \nabla \ln s \quad (1)$$

\* mamta.jotkar@upm.es, mamta.jotkar@idaea.csic.es

† pietro.deana@unil.ch

‡ marco.dentz@idaea.csic.es

§ luis.cueto@upm.es

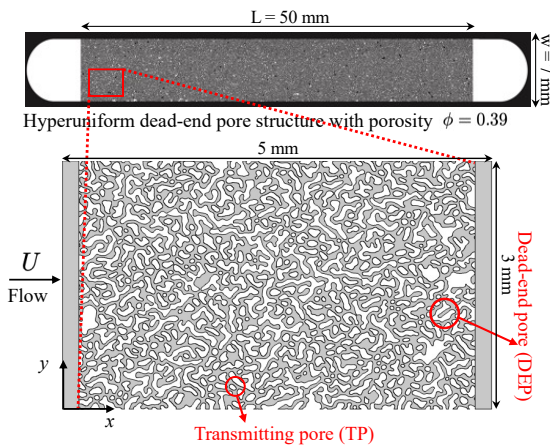


FIG. 1. Hyper-uniform porous structure characterized by DEPs and TPs. Computational domain with white spaces indicating solid grains (bottom).

and the diffusiophoretic mobility  $\Gamma_p$  is approximately a constant.  $\Gamma_p$  is determined by the size and surface charge of the particle [2, 3]

$$\Gamma_p = \frac{\varepsilon k_B T}{\nu Z e} \left\{ D\zeta - \frac{2k_B T}{Ze} \ln \left[ 1 - \tanh^2 \left( \frac{Ze\zeta}{4k_B T} \right) \right] \right\},$$

where  $\varepsilon$  is the dielectric permittivity of the medium,  $\zeta$  is the particle zeta potential,  $\nu$  is the kinematic viscosity of the medium,  $k_B$  is the Boltzmann constant,  $T$  is the absolute temperature,  $Z$  is the valence of the constituent ions of the solute,  $e$  is the proton charge and  $D = (D_+ - D_-)/(D_+ + D_-)$  measures the difference in diffusivity  $D_+$  of the cation and  $D_-$  of the anion. The logarithmic dependence of the particle velocity  $\mathbf{u}_{dp}$  on the solute concentration gradients  $\nabla s$  allows for rapid and efficient particle motion, even in low concentration areas.

We consider a porous system characterized by DEPs of different size connected to a network of TPs, similar to the one used in ref. [28]. The computational domain is shown in figure 1. The mean flow is driven from left to right with the flow rate  $U$ . The medium is statistically homogeneous with a mean pore-size  $\lambda = 30\mu\text{m}$  and porosity  $\phi = 0.39$ . The dual feature of this medium is characterized by TPs, and DEPs leading to stagnant flow. While solutes typically diffuse and dissipate gradients within pores over time scales shorter than the time  $\tau_L = L/U$  needed to elute a pore-volume, the junctures of TPs and DEPs serve as excellent candidates to retain gradients of solute concentration, which in turn trigger DP.

In the low Reynolds number limit, the fluid-solute-particle dynamics are governed by the Stokes equation for fluid flow, and the advection-diffusion equations for the solute and particle transport [5]

$$0 = \frac{1}{\rho} (-\nabla p + \mu \nabla^2 \mathbf{u}), \quad (2a)$$

$$\nabla \cdot \mathbf{u} = 0, \quad (2b)$$

$$\frac{\partial s}{\partial t} + \nabla \cdot (\mathbf{u}s) = D_s \nabla^2 s, \quad (2c)$$

$$\frac{\partial c}{\partial t} + \nabla \cdot (\mathbf{u} + \mathbf{u}_{dp})c = D_p \nabla^2 c, \quad (2d)$$

where  $\mathbf{u}$  is the two-dimensional velocity field,  $p$  is the pressure,  $s$  is the solute concentration and  $c$  is the particle concentration,  $\mu$  is the dynamic viscosity of the fluid and  $\rho$  its density.  $D_s$  and  $D_p$  are the diffusion coefficient of solute and particles, respectively. Typically, solutes diffuse much faster than particles such that  $D_s \gg D_p$ . Solute and particle transport can be characterized by the respective Péclet numbers,  $Pe_s = U\lambda/D_s$  and  $Pe_p = U\lambda/D_p$ , which compare the characteristic diffusion time scales  $\tau_{D_s} = \lambda^2/D_s$  and  $\tau_{D_p} = \lambda^2/D_p$  to the advection time  $\tau_v = \lambda/U$  over the mean pore length. The diffusiophoretic particle velocity  $\mathbf{u}_{dp}$  is given by Eq.(1). The medium is initially saturated with particles and solute with initial concentrations  $c_i$  and  $s_i$ , respectively. At time  $t > 0$ , a sharp front of solute at concentration  $s_H \gg s_i$  is injected such that the ratio  $\chi = s_i/s_H \ll 1$ . This solute front induces a dynamic and heterogeneous solute concentration gradient that drives DP. The governing equations (2) are solved numerically for the pore geometry detailed above. The numerical setup is described in [32].

Figure 2 shows the temporal evolution of the particle concentration field without DP ( $\Gamma_p = 0$ ), and for diffusiophoretic trapping ( $\Gamma_p < 0$ ), and extraction ( $\Gamma_p > 0$ ). In the absence of DP, majority of the particles get dispersed through the TPs leaving behind a small fraction of particles that accumulate within the DEPs, where the flow is stagnant, organized in convection rolls [28]. The only mechanism through which these localized particles can escape into the TPs is diffusion, the times scale of which is typically orders of magnitude larger than  $\tau_L$ .

The injection of a sharp front of solute at a higher concentration results in local gradients of solute concentration that drive DP within the DEPs. For  $\Gamma_p < 0$ , that is, when particles migrate from high to low solute concentrations, DP leads to the trapping of particles inside the DEPs, as shown in figure 2(a).

When  $\Gamma_p > 0$ , DP leads to particle mobilization out of the DEPs because the particles move towards the higher solute concentration zones in the TPs. This is seen in the particle distributions shown in Figure 2(c), where the particles within the DEPs rapidly escape the DEPs and leave the domain from the right outlet. Figure 3 shows the time evolution of the solute concentration at a point within a DEP close to the bottom of the DEP. The increase or decrease of concentration due to DP occurs on the time scale  $\tau_{D_s}$ , which here is smaller than  $\tau_{D_p}$  by a factor of  $10^3$ . Thus, the action of DP on mass transfer between TPs and DEPs is limited to relatively short initial times.

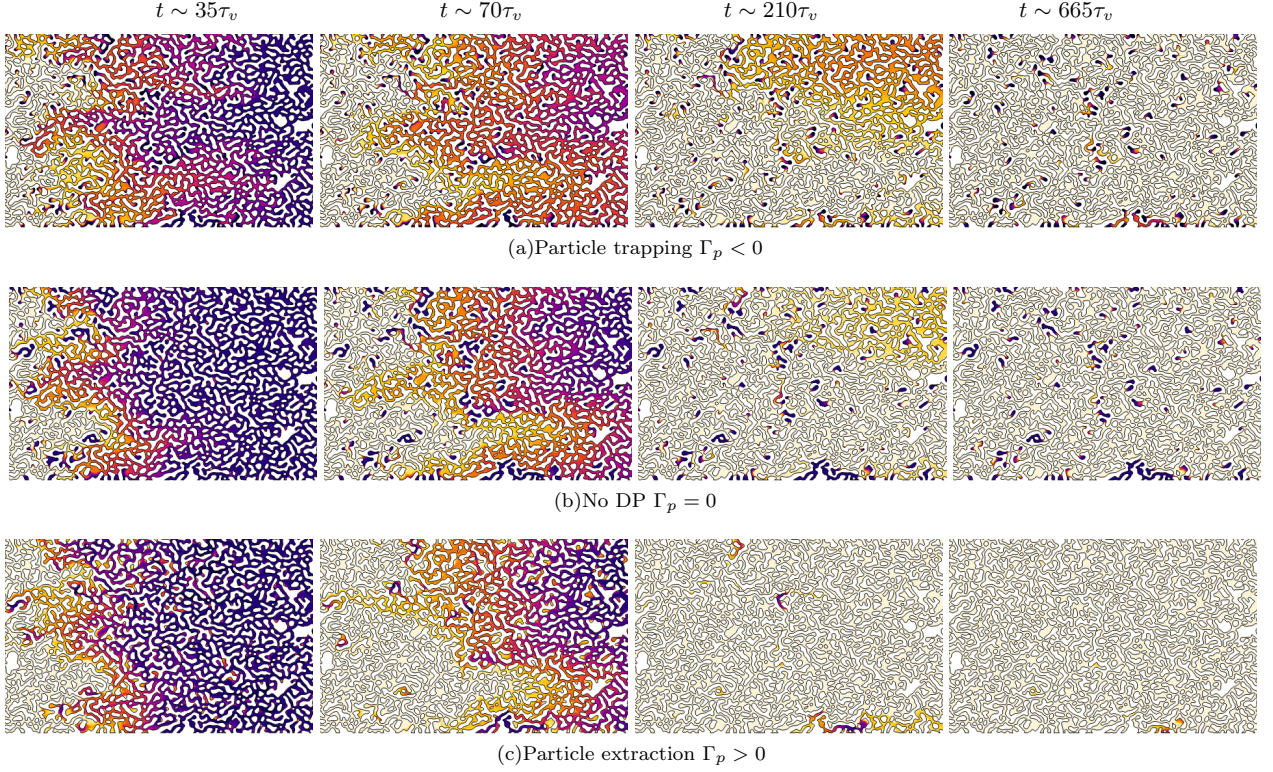


FIG. 2. Temporal evolution of the dimensionless particle distributions  $c/c_i$  for (a) trapping, (b) no-DP, and (c) extraction cases. The concentration scale is logarithmic between  $10^{-5}$  (light) and 10 (dark). White spaces indicate solid grains.

To understand how DP controls the macroscopic fate of the suspended particles, we first estimate the fraction  $\alpha$  of particles that are trapped in or mobilized from the DEPs in the initial phase. To this end, we consider a single DEP connected to a TP [32]. For this geometry, we can derive

the solute concentration profile in the DEP, and thus obtain explicit expressions for the diffusiophoretic drift  $u_{dp}$ . Combining the latter with conservation of particle flux at the interface between TP and DEP, we obtain the following expression for  $\alpha$  as a function of  $\Gamma_p^* = \Gamma_p/U\lambda$

$$\alpha = \alpha_0 [1 - \Gamma_p^*(1 - \chi)Pe_s] + H(-\Gamma_p^*) \left\{ \frac{2\Gamma_p^{*2}(1 - \chi)^2 Pe_s Pe_p \ell_0^*}{\pi} \ln \left[ \frac{2\Gamma_p^*(1 - \chi) Pe_p \ell_0^*}{2\Gamma_p^*(1 - \chi) Pe_p \ell_0^* - \pi} \right] \right\}, \quad (3)$$

where  $H(\cdot)$  is the Heaviside step function, and  $\alpha_0$  the initial fraction of particles in the DEPs in the absence of DP ( $\Gamma_p = 0$ ). The dimensionless length  $\ell_0^*$  denotes a characteristic diffusion scale at the interface between TP and DEP. It is inversely proportional to the particle Péclet number,  $\ell_0^* \sim 1/Pe_p$ . We set in the following  $\ell_0^* = \beta/Pe_p$  with  $\beta$  a number of the order of one. Expression (3) predicts that the particles are depleted from the DEPs for  $\Gamma_p^* \geq 1/(1 - \chi)Pe_s$ . Furthermore, for strongly negative diffusiophoretic mobility, the rate at which particles are transferred to the interface is eventually smaller than the diffusiophoretic drift. Thus, by taking the limit of  $\Gamma_p^* \rightarrow -\infty$  in Eq. (3), we find that  $\alpha$  asymptotes

toward

$$\alpha_\infty = \alpha_0 \left( 1 + \frac{\pi Pe_s}{\beta} \right). \quad (4)$$

The trapped particle fraction increases linearly with  $Pe_s$  because the solute gradients and thus the diffusiophoretic drift increase with increasing  $Pe_s$ .

Figure 4 shows the distribution of arrival times of particles at the outlet. Similar to Ref. [28], we observe two transport regimes. At times of the order of  $\tau_L$ , particles at the outlet are produced by advection and dispersion from the TPs. For times  $t \gg \tau_L$ , the arrival time distribution deviates from the exponential decay predicted

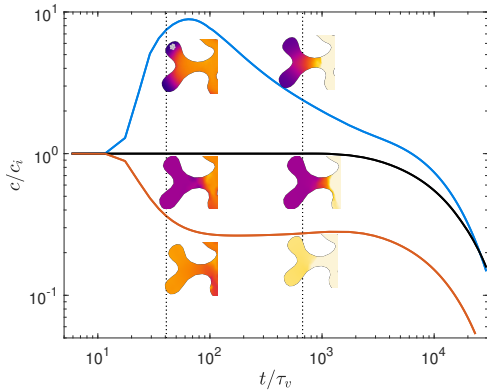


FIG. 3. Temporal evolution of dimensionless particle concentration ( $c/c_i$ ) at an arbitrary point (indicated by grey) within a DEP shown in the inset for  $\Gamma_p^* = -1$  (blue, trapping),  $\Gamma_p^* = 0$  (black, no DP), and  $\Gamma_p^* = 0.4$  (red, extraction). The particle concentrations shown in the inset are displayed in a logarithmic scale and range from  $10^{-6}$  (light) to 10 (dark).

under the classical dispersion framework and displays a power law tail. This is caused by the particles that are initially trapped within the DEPs. For  $\Gamma_p < 0$ , an increasing fraction of particles is trapped in the DEP, which manifests in a stronger tail than without DP. For  $\Gamma_p > 0$ , particles are extracted from the DEP at initial times, and thus the tail is weaker than for  $\Gamma_p \leq 0$ .

The arrival time distribution can be modeled as the superposition of the residence time distributions in the TPs and DEPs [28]

$$F(t) = (1 - \alpha)F_0(t) + \alpha \int_0^\infty d\tau \frac{g(t/\tau)}{\tau} f_D(\tau), \quad (5)$$

respectively. Note that  $\alpha$  is the fraction of trapped particles after the short initial phase, which can be approximated by expression (3). We assume that transport in the TP can be characterized by the mean flow velocity and a hydrodynamic dispersion coefficient. Thus,  $F_0(t)$  is given by the superposition of inverse Gaussian distributions as,

$$F_0(t) = \frac{1}{L} \int_0^L dx \frac{x \exp[-(x - \bar{u}t)^2/(4D_h t)]}{\sqrt{4\pi D_h t^3}}. \quad (6)$$

As we see in Figure 4, this approximation is able to capture the early arrival times, but underestimates the arrival time distribution at intermediate times. This can be traced back to the velocity variability between pores [31]. The residence time distribution within the DEPs is expressed in terms of a Gamma-distribution  $g(t')$  of dimensionless residence times  $\tau' = \tau/\tau_{D_p}$  in a single DEP and

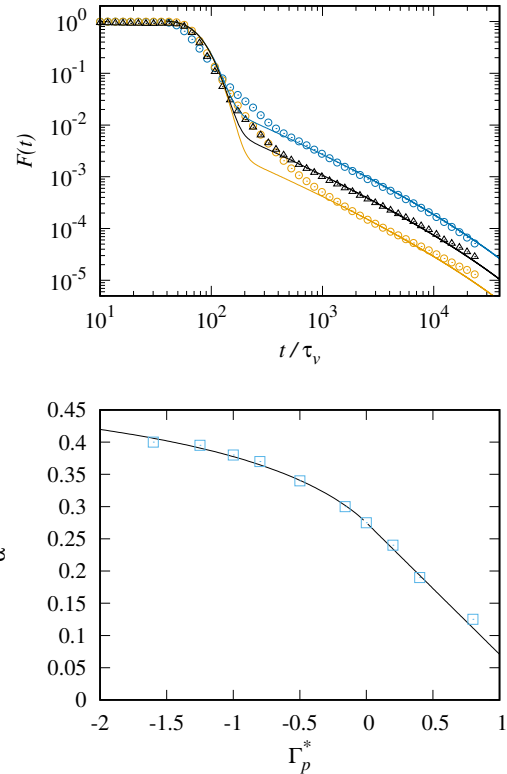


FIG. 4. (Top panel) Arrival time distribution  $F(t)$  at the outlet for (blue circles)  $\Gamma_p^* = -1$ , (black triangles) 0 and (orange circles) 0.4. The solid lines denote the travel-time model in Eq. (5). (Bottom panel) Particle fraction  $\alpha$  in the DEP from the (symbols) numerical data, and (solid line) the analytical expression (3) for  $\ell_0^* = 0.65/Pe_p$ .

the distribution  $f_D$  of characteristic diffusion times  $\tau_{D_p}$ , given below [28]

$$g(t') = \frac{t'^{-2/3} \exp(-t')}{\Gamma(1/3)}, \quad (7)$$

while  $f_D$  is obtained from the distribution  $f_\Lambda$  of aspect ratios  $\Lambda$  through the map  $\Lambda \rightarrow \tau_{D_p} = (\lambda\Lambda)^2/D_p$ .

Figure 4 shows the numerically estimated particle fractions versus the dimensionless diffusio-phoretic mobility, and the analytical expression (3) for  $\beta = 0.65$ . The analytical model describes the full dependence of  $\alpha$  on  $\Gamma_p$  for both extraction from and trapping in DEPs, and thus seems to capture the controls of DP on the macro-scale dispersion of particles.

In conclusion, the microscopic interactions between DP and flow and transport through porous media impact the macroscopic fate of particles. Depending on the diffusio-phoretic mobility  $\Gamma_p$ , DP may promote trapping within or it may lead to particle mobilization from the DEPs. This can be exploited for preferential particle deposition

or removal. DP is a short-term phenomenon that persists as long as the solute gradients are not dissipated by diffusion, which is characterized by the time scale  $\tau_{D_s} = \lambda^2/D_s$  and is typically smaller than the characteristic advection time across the medium i.e.  $\tau_{D_s} \ll \tau_L$ . However, despite its short timespan, DP has a significant impact on macroscopic transport, by reorganizing the partitioning of particles between the DEPs and TPs, which is quantified by the fraction  $\alpha$ .

Our results suggest that DP provides an efficient way of controlling particle transport through porous media in a reversible manner by changing the direction of the solute gradient. Moreover, the existence of DEPs is quite common in natural geological and biological porous media, and serve as excellent candidates for retaining microscopic gradients of solute concentration for relatively large times. This opens new avenues for developing tech-

nological solutions to various problems of socio-economic relevance such as groundwater remediation, enhanced oil recovery, water-filtration systems, targeted drug delivery and microfluidics for biomedical applications.

## ACKNOWLEDGMENTS

This work has received funding from European Union's Horizon 2020 research and innovation program under the Marie Skłodowska-Curie G.A. No. 895569. MD and LCF gratefully acknowledge funding from the Spanish Ministry of Science and Innovation through the project HydroPore (PID2019-106887GB-C31-C33). P.d.A. acknowledges the support of FET-Open project NARCISO (ID: 828890) and of Swiss National Science Foundation (grant ID 200021 172587).

- 
- [1] B. V. Derjaguin, G. P. Sidorenkov, E. A. Zubashchenkov, and E. V. Kiseleva. Kinetic phenomena in boundary films of liquids. *Colloid J. USSR*, 9:335–347, 1947.
- [2] D. C. Prieve, J. L. Anderson, J. P. Ebel, and M. E. Lowell. Motion of a particle generated by chemical gradients. part 2. Electrolytes. *J. Fluid Mech.*, 148:247–269, 1984.
- [3] J. L. Anderson. Colloid transport by interfacial forces. *Annu. Rev. Fluid Mech.*, 21(1):61–99, 1989.
- [4] D. Velegol, A. Garg, R. Guha, A. Kar, and M. Kumar. Origins of concentration gradients for diffusiophoresis. *Soft Matter*, 12:4686–4703, 2016.
- [5] J. T. Ault, S. Shin, and H. A. Stone. Diffusiophoresis in narrow channel flows. *J. Fluid Mech.*, 854:420–448, 2018.
- [6] B. Abécassis, C. Cottin-Bizonne, C. Ybert, A. Ajdari, and L. Bocquet. Boosting migration of large particles by solute contrasts. *Nat. Mater.*, 7(10):785–789, 2008.
- [7] J. Palacci, B. Abécassis, C. Cottin-Bizonne, C. Ybert, and L. Bocquet. Colloidal motility and pattern formation under rectified diffusiophoresis. *Phys. Rev. Lett.*, 104:138302, 2010.
- [8] A. Kar, T.-Y. Chiang, I. Ortiz Rivera, A. Sen, and D. Velegol. Enhanced transport into and out of dead-end pores. *ACS Nano*, 9(1):746–753, 2015. PMID: 25559608.
- [9] S. Shin, E. Um, B. Sabass, J. T. Ault, M. Rahimi, P. B. Warren, and H. A. Stone. Size-dependent control of colloid transport via solute gradients in dead-end channels. *Proc. Natl. Acad. Sci.*, 113(2):257–261, 2016.
- [10] S. Battat, J. T. Ault, S. Shin, S. Khodaparast, and H. A. Stone. Particle entrainment in dead-end pores by diffusiophoresis. *Soft Matter*, 15:3879–3885, 2019.
- [11] N. Singh, Goran T. Vladislavljević, Fran çois Nadal, Cécile Cottin-Bizonne, Christophe Pirat, and Guido Bolognesi. Reversible trapping of colloids in microgrooved channels via diffusiophoresis under steady-state solute gradients. *Phys. Rev. Lett.*, 125:248002, 2020.
- [12] Nan Shi, Rodrigo Nery-Azevedo, Amr I. Abdel-Fattah, and Todd M. Squires. Diffusiophoretic focusing of suspended colloids. *Phys. Rev. Lett.*, 117:258001, 2016.
- [13] Shin S., Shardt O., Warren P. B., and Stone H. A. Membraneless water filtration using  $CO_2$ . *Nat. Commun.*, 8:15181, 2017.
- [14] S. Shin, P. B. Warren, and H. A. Stone. Cleaning by surfactant gradients: Particulate removal from porous materials and the significance of rinsing in laundry detergency. *Phys. Rev. Appl.*, 9:034012, 2018.
- [15] M. K. Rasmussen, J. N. Pedersen, and R. Marie. Size and surface charge characterization of nanoparticles with a salt gradient. *Nat. Commun.*, 11(1):2337, 2020.
- [16] Jotkar M. and Cueto-Felgueroso L. Particle separation through diverging nanochannels via diffusiophoresis and diffusioosmosis. *Phys. Rev. Applied*, 16:064067, 2021.
- [17] P. O. Staffeld and J. A. Quinn. Diffusion-induced banding of colloid particles via diffusiophoresis: 1. Electrolytes. *J. Colloid Interface Sci.*, 130(1):69–87, 1989.
- [18] J. Bear. *Dynamics of fluids in porous media*. Courier Corporation, 1988.
- [19] David M. Kahler and Zbigniew J. Kabala. Acceleration of groundwater remediation by rapidly pulsed pumping: Laboratory column tests. *Journal of Environmental Engineering*, 145(1):06018009, 2019.
- [20] S. Thomas. *Oil and Gas Science and Technology - Rev. IFFP*, 63 (1):9–19, 2008.
- [21] Liang Lei, Taehyung Park, Karl Jarvis, Lingli Pan, Imgenur Tepecik, Yumeng Zhao, Zhuan Ge, Jeong-Hoon Choi, Xuerui Gai, Sergio Andres Galindo-Torres, Ray Boswell, Sheng Dai, and Yongkoo Seol. Pore-scale observations of natural hydrate-bearing sediments via pressure core sub-coring and micro-ct scanning. *Scientific Reports*, 12(3471).
- [22] F. Miele, P. de Anna, and M. Dentz. Stochastic model for filtration by porous materials. *Phys. Rev. Fluids*, 4:094101, 2019.
- [23] Lever D.A., Bradbury M.H., and Hemingway S.J. The effect of dead-end porosity on rock-matrix diffusion. *Journal of Hydrology*, 80:45–76, 1985.
- [24] Naoki Nishiyama and Tadashi Yokoyama. Permeability of porous media: Role of the critical pore size. *Journal of Geophysical Research: Solid Earth*, 122(9):6955–6971, 2017.
- [25] Amandine Erktan, Dani Or, and Stefan Scheu. The physical structure of soil: Determinant and consequence of trophic interactions. *Soil Biology and Biochemistry*,

- 148:107876, 2020.
- [26] Siegfried Hapfelmeier, Melissa A. E. Lawson, Emma Slack, Jorum K. Kirundi, Maaïke Stoel, Mathias Heikenthalder, Julia Cahenzli, Yuliya Velykoredko, Maria L. Balmer, Kathrin Endt, Markus B. Geuking, Roy Curtiss, Kathy D. McCoy, and Andrew J. Macpherson. Reversible microbial colonization of germ-free mice reveals the dynamics of iga immune responses. *Science*, 328(5986):1705–1709, 2010.
- [27] William A. Phillip, Rachel Mika Dorin, Jörg Werner, Eric M. V. Hoek, Ulrich Wiesner, and Menachem Elimlech. Tuning structure and properties of graded triblock terpolymer-based mesoporous and hybrid films. *Nano Letters*, 11(7):2892–2900, 2011. PMID: 21648394.
- [28] A. D. Bordoloi, D. Scheidweiler, M. Dentz, Bouabdel-laoui M., Abbarchi M., and de Anna P. Structure induced laminar vortices control anomalous dispersion in porous media. *Nat. Commun.*, 13:3820, 2022.
- [29] Dentz Marco, Le Borgne Tanguy, Englert Andreas, and Bijeljic Branko. Mixing, spreading and reaction in heterogeneous media: A brief review. *Journal of Contaminant Hydrology*, 120-121:1–17, 2011.
- [30] P. de Anna, B. Quaife, G. Biros, and R. Juanes. Prediction of velocity distribution from pore structure in simple porous media. *Phys. Rev. Fluids*, 2:124103, 2017.
- [31] M. Dentz, M Icardi, and J. J. Hidalgo. Mechanisms of dispersion in a porous medium. *J. of Fluid Mech.*, 841:851–882, 2018.
- [32] See Supplemental Material at [*URL will be inserted by publisher*] for the setup of the detailed numerical simulations and the details on the analytical model.

# Supplemental Material: Diffusiophoresis and medium structure control macroscopic particle transport in porous media

Mamta Jotkar\*

*Universidad Politécnica de Madrid, Spain,  
Institute of Environmental Assessment and Water Research,  
Spanish National Research Council, Barcelona, Spain*

Pietro de Anna†

*Institute of Earth Sciences, University of Lausanne, Switzerland*

Marco Dentz‡

*Institute of Environmental Assessment and Water Research,  
Spanish National Research Council, Barcelona, Spain*

Luis Cueto-Felgueroso§

*Universidad Politécnica de Madrid, Spain*

(Dated: March 16, 2023)

This supplemental material gives details on the setup of the detailed numerical simulations of flow and solute and particle transport, and the derivation of the one-dimensional analytical model for the quantification of the fraction of particles trapped in the DEPs.

Keywords: Diffusiophoresis, anomalous dispersion, porous media

## I. NUMERICAL SIMULATIONS

The computational domain is shown in figure 1 in the main text. The mean flow is from left to right. This medium is statistically homogeneous such that the distribution of the pore-size is narrow with a strong peak close to mean pore-size  $\lambda = 30\mu\text{m}$ . It exhibits complex pore network interspersed among disordered solid grains with a porosity  $\phi = 0.39$ . The domain is initially saturated with solute at a lower concentration ( $s_i = 0.1\text{mM}$ ) and particles. A sharp front of solute at a higher concentration ( $s_H = 10\text{mM}$ ) is then injected such that the ratio  $\chi = s_i/s_H = 0.01$ . The governing equations (Eq.(2) in the article) are subjected to no slip and no penetration flow at the solid surfaces, uniform flow with an average fluid speed  $U$  at the left inlet and constant pressure at the right outlet. For the solute concentration, we use constant flux at the inlet and no flux boundary condition everywhere else whereas, for the particle concentration, we impose a conservative form of no flux boundary condition, where the sum of diffusive and advective fluxes is zero. As an initial condition, we assume initially no flow  $\mathbf{u} = 0, p = 0$  and impose solute concentration  $s_i = 0.1\text{mM}$  and particle concentration  $c_i = 0.1\text{mM}$ . The numerical model has been validated for a simpler micro-channel geometry [1] as well as for the hyper-uniform porous medium considered here by approximating the case without DP with Ref. [2]. We use COMSOL Multiphysics® based on finite element for performing the pore-scale simulations [3]. For the physical parameters we use the following values (closest to realistic ones):  $\mu = 10^{-3}\text{Pa}\cdot\text{s}$ ,  $\rho = 10^3\text{kg}/\text{m}^3$ ,  $D_s = 7 \times 10^3\mu\text{m}^2/\text{s}$ ,  $D_p = 7\mu\text{m}^2/\text{s}$  and  $U = 175\mu\text{m}/\text{s}$ . This yields a characteristic advection time of  $\tau_v = 0.17\text{ s}$ , the salt diffusion time  $\tau_{D_s} = 0.12\text{ s}$ , the particle diffusion time  $\tau_{D_p} = 128\text{ s}$ , and the Péclet numbers  $Pe_s = U\lambda/D_s = 0.75$  based on the solute and  $Pe_p = U\lambda/D_p = 750$  based on the particles. Particle concentrations at the outlet for different mobilities  $\Gamma_p$  are shown in figure 1.

## II. ANALYTICAL MODEL

We construct a one-dimensional model to quantify the dependence of the initial fraction of particles  $\alpha$  within the DEPs on the DP mobility  $\Gamma_p$  (see figure 2). To this end, we assume that particle transport in the DEP at short times

---

\* mamta.jotkar@upm.es, mamta.jotkar@idaea.csic.es

† pietro.deana@unil.ch

‡ marco.dentz@idaea.csic.es

§ luis.cueto@upm.es

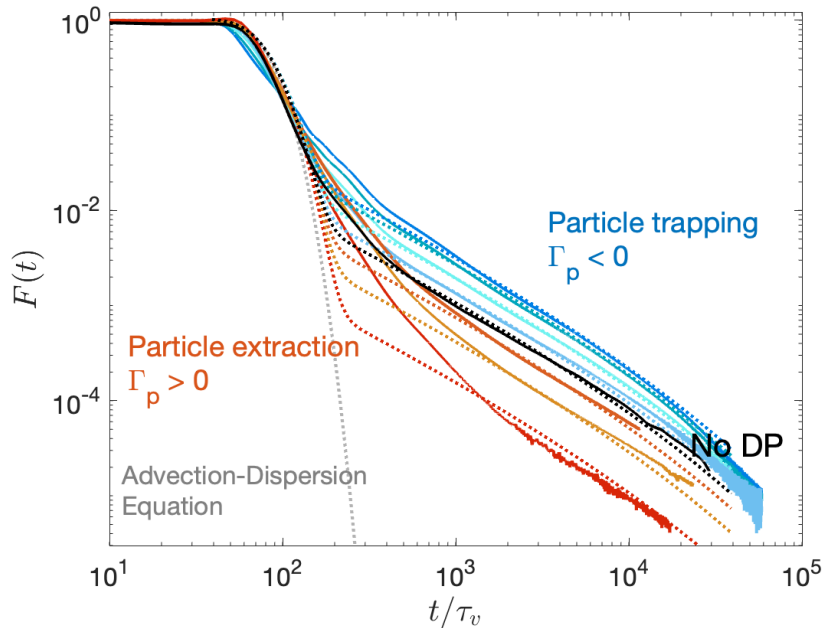


FIG. 1. Numerical simulations. Arrival time distribution at the outlet for different diffusiophoretic mobilities  $\Gamma_p/\lambda U$  ranging from -1.6, -1, -0.5, -0.01 (shades of blue, trapping) to 0 (black, no DP) to 0.02, 0.4, 0.8 (shades of red, extraction). Solid curves correspond to numerical simulations while dotted curves correspond to the one-dimensional travel-time model obtained using different fraction  $\alpha$  of particles initially available within the DEPs.

is dominated by the diffusiophoretic drift such that

$$\frac{\partial c}{\partial t} + \frac{\partial}{\partial x} u_{dp} c = 0. \quad (1)$$

The total mass of particles in the DEP is given by

$$m_{dp} = w \int_0^{\ell_p} dx c, \quad (2)$$

where  $w$  is the pore-width. Since the only flux of particles toward or from the DEP is across the DEP-TP junction, the temporal variability of the mass of particles in the DEP is equal to the mass flux at  $x = 0$  and controlled by DP. Spatial integration of Eq. (1) according to Eq. (2) gives

$$\frac{\partial m_{dp}}{\partial t} = w u_{dp}(x = 0, t) c(x = 0, t), \quad (3)$$

where we used that there is no flux across the boundary at  $x = \ell_p$ . Thus, the added or extracted mass is given by

$$m_{dp} = m_i + w \int_0^{\infty} dt u_{dp}(x = 0, t) c(x = 0, t). \quad (4)$$

In the following, we first determine the diffusiophoretic drift, then we deal with the cases of extraction ( $\Gamma_p > 0$ ) and addition of particles ( $\Gamma_p < 0$ ) separately.



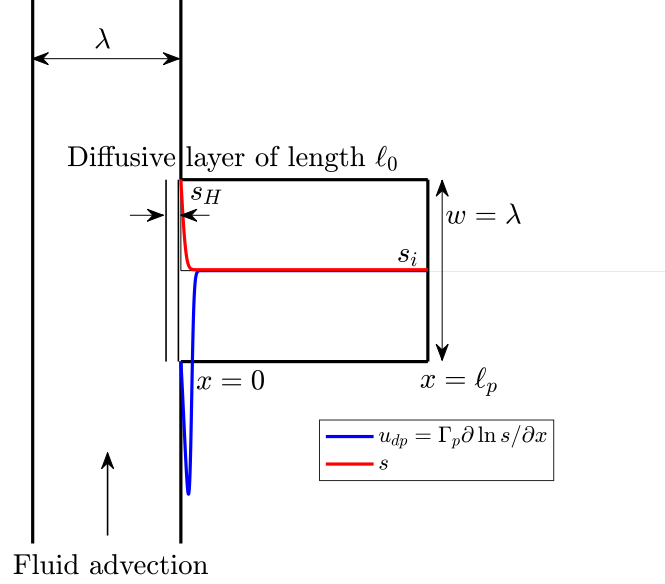


FIG. 2. Illustration of the one-dimensional analytical model. A single DEP of length  $\ell_p$  is connected to a (vertical) TP with a width of  $\lambda$ . The solute concentration within the DEP is illustrated by the red line, the blue line denotes the profile of  $u_{dp}$ . At short times, the diffusiophoretic drift is strongly localized at the interface between TP and DEP.

### A. Diffusiophoretic drift

We focus here on estimating the drift  $u_{dp}$ . The Péclet number for salt is so low that we can assume that diffusion dominates in the DEP. Thus, to obtain the salt concentration  $s$ , we solve the diffusion equation

$$\frac{\partial s}{\partial t} - D_s \frac{\partial^2 s}{\partial x^2} = 0. \quad (5)$$

We consider the boundary conditions  $s = s_H$  at  $x = 0$  and  $\partial s / \partial x = 0$  at  $x = L$ . The initial condition is  $s(x, t = 0) = s_i$ . In Laplace space we obtain the exact solution

$$s^*(x, \sigma) = \frac{s_i}{\sigma} + \frac{(s_H - s_i) \cosh[(1 - x/\ell_p)\sqrt{\sigma\tau_{D_s}}]}{\sigma \cosh(\sqrt{\sigma\tau_{D_s}})}, \quad (6)$$

where  $\tau_{D_s} = \ell_p^2 / D_s$  and  $\sigma$  is the Laplace variable. The Laplace transform is defined in [4].

The Laplace transform of the diffusiophoretic velocity at  $x = 0$  is then given by

$$u_{dp}^*(x = 0, \sigma) = -\Gamma_p(1 - \chi) \frac{\tanh(\sqrt{\sigma\tau_{D_s}})}{\sqrt{\sigma D_s}}, \quad (7)$$

where we defined  $\chi = s_i / s_H$ . The integral of the drift from  $t = 0$  to  $\infty$  is given by

$$\int_0^\infty dt u_{dp}(x = 0, t) = u_{dp}^*(x = 0, \sigma = 0) = -\frac{\Gamma_p(1 - \chi)\ell_p}{D_s}. \quad (8)$$

This expression is used directly to estimate the total mass of trapped particles for the extraction case, as argued below. For the trapping case, however, the full time dependence of  $u_{dp}(, 0, t)$  is required as can be seen from Eq. (4). Thus, we approximate the salt concentration profile in the DEP by the solution for a semi-infinite domain,

$$s^a(x, t) = s_i + (s_H - s_i) \operatorname{erfc}(x / \sqrt{4D_s t}), \quad (9)$$

where the superscript  $a$  denotes approximation. Using this expression, the diffusiophoretic drift is given by

$$u_{dp}^a(x, t) = -\Gamma_p(s_H - s_i) \frac{\exp(-x^2/4D_s t)}{s(x, t)\sqrt{\pi D_s t}}. \quad (10)$$

The drift at  $x = 0$  then is given by

$$u_{dp}^a(x = 0, t) = -\frac{\Gamma_p(1 - \chi)}{\sqrt{\pi D_s t}}, \quad (11)$$

where we used that  $s(x = 0, t) = s_H$ . For times larger than  $\tau_{D_s} = \ell_p^2/D_s$ , the salt gradient decays exponentially fast with time. Thus, the time integral over the drift can be written as

$$\int_0^\infty dt u_{dp}(x = 0, t) = \int_0^{\tau_{D_s}^a} dt u_{dp}^a(x = 0, t) = -\sqrt{\frac{4}{\pi a}} \frac{\Gamma_p(1 - \chi)\ell_p}{\sqrt{D_s}}. \quad (12)$$

In order to match the exact expression (8), we set  $a = \pi/4$  and use the following the approximation

$$u_{dp}^a(x = 0, t) = -\frac{\Gamma_p(1 - \chi)}{\sqrt{4\pi D_s t}} H(\tau_{D_s}\pi - t), \quad (13)$$

where  $H(t)$  denotes the Heaviside step function.

### B. Extraction of particles

In the case  $\Gamma_p > 0$ , particles are extracted from the DEP. The particle concentration at  $x = 0$ , that is, at the interface with the TP is set equal to  $c(x = 0, t) = c_i$ , the resident particle concentration. Thus, we obtain by integration of Eq. (3) for the added particle mass

$$m_{dp} = m_i + c_i w \int_0^\infty dt u_{dp}(x = 0, t) = m_i + c_i w u_{dp}^*(x = 0, \sigma = 0) = m_i - \frac{m_i \Gamma_p (1 - \chi)}{D_s}, \quad (14)$$

where  $m_i = c_i w \ell_p$  is the initial particle mass and  $\chi = s_i/s_H$ . Note that we used expression (8) to arrive at this result. If  $\alpha_0$  is the fraction of particle mass inside the DEP without DP, then the fraction  $\alpha$  of particles after DP is

$$\alpha = \alpha_0 \frac{m_{dp}}{m_i}. \quad (15)$$

Using Eq. (14) and setting  $\ell_p = \lambda$ , we obtain

$$\alpha = \alpha_0 [1 - \Gamma_p^* P e_s (1 - \chi)], \quad (16)$$

where  $\Gamma_p^* = \Gamma_p/\lambda U$  is the dimensionless form of the diffusiophoretic mobility and  $P e_s = \lambda U/D_s$  is the salt Péclet number.

### C. Trapping of particles

In the case  $\Gamma_p < 0$ , particles are trapped from the TP into the DEP. In order to determine  $c(x = 0, t)$ , we consider the balance of fluxes across the interface. For  $x < 0$ , that is within the TP, the particle flux transverse to the flow direction is due to diffusion. For  $x > 0$ , that is, in the DEP the particle flux is dominated by the diffusiophoretic drift. Thus, we can write

$$-D_p \frac{c(x = 0, t) - c_i}{\ell_0} = u_{dp}(x = 0, t) c(x = 0, t), \quad (17)$$

where  $\ell_0$  is the concentration gradient scale. We assume that the particle concentration in the flow past the interface between TP and DEP is constant and equal to the initial concentration  $c_i$ . We estimate  $\ell_0$  as the length scale at

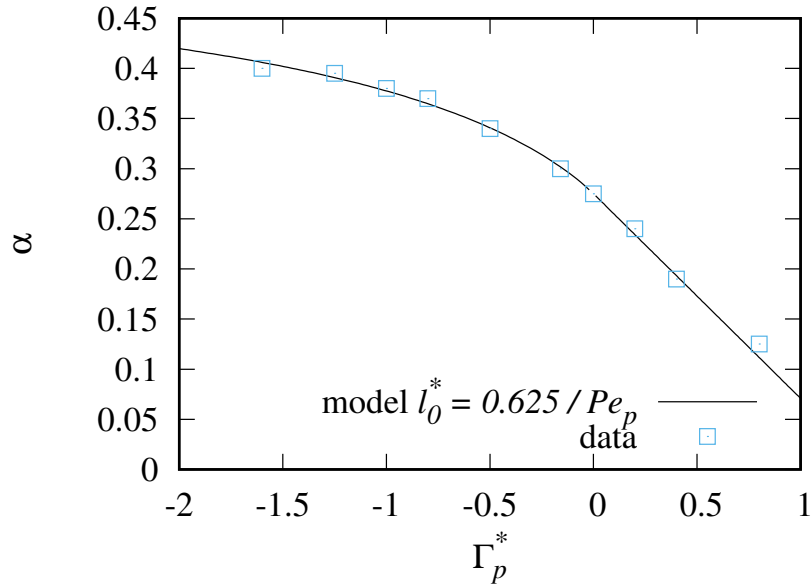


FIG. 3. Data for the dependence of  $\alpha$  on  $\Gamma_p^*$  (symbols) and the analytical model (solid line) for  $Pe_s = 0.75$ ,  $Pe_p = 750$  and  $\ell_0^* = 0.65/Pe_p$ .

which the diffusive flux transverse to the flow direction toward the interface is of the same order as the advective flux past the interface, that is,

$$Uc_i \sim D_p \frac{c_i}{\ell_0}. \quad (18)$$

From this relation, we obtain the estimate

$$\ell_0 \sim \frac{D_p}{U} = \frac{\ell_p}{Pe_p}. \quad (19)$$

That is, particles within the layer of thickness  $\ell_0$  are available for trapping in the DEP. From (17), we obtain for  $c_0(t) \equiv c(x=0, t)$

$$c_0(t) = \frac{c_i}{1 + \frac{u_0(t)\ell_0}{D_p}}, \quad (20)$$

where we set  $u_0(t) = u_{dp}(x=0, t)$ . Inserting (20) into (4) gives

$$m_{dp} = m_i + w \int_0^\infty dt u_0(t) \frac{c_i}{1 + \frac{u_0(t)\ell_0}{D_p}}. \quad (21)$$

Note that here use the approximation (13) for  $u_0(t)$  to derive an analytical expression for  $m_{dp}$ .

Inserting expression (13) into the right side of Eq. (21) gives

$$m_{dp} = m_i + w \int_0^{\tau_{D_s} \pi/4} dt \frac{\hat{\Gamma}_p(1-\chi)}{\sqrt{\pi D_s t}} \frac{c_i}{1 + \frac{\hat{\Gamma}_p(1-\chi)\ell_0}{\sqrt{\pi D_s t} D_p}}. \quad (22)$$

where we set  $\hat{\Gamma}_p = -\Gamma_p$ . We can further write

$$m_{dp} = m_i + wc_i \int_0^{\tau_{D_s} \pi/4} dt \frac{\hat{\Gamma}_p(1-\chi)}{\sqrt{\pi D_s t} + \frac{\hat{\Gamma}_p(1-\chi)\ell_0}{D_p}}. \quad (23)$$

Integration of the latter gives

$$m_{dp} = m_i + w\ell_p c_i \left\{ \frac{\hat{\Gamma}_p(1-\chi)}{D_s} + \frac{2\hat{\Gamma}_p^2(1-\chi)^2\ell_0}{\pi D_s D_p \ell_p} \ln \left[ \frac{2\hat{\Gamma}_p(1-\chi)}{2\hat{\Gamma}_p(1-\chi) + \pi D_p \ell_p / \ell_0} \right] \right\} \quad (24)$$

Thus, we obtain for  $\alpha$

$$\alpha = \alpha_0 \left\{ 1 + \frac{\hat{\Gamma}_p(1-\chi)}{D_s} + \frac{2\hat{\Gamma}_p^2(1-\chi)^2\ell_0}{\pi D_s D_p \ell_p} \ln \left[ \frac{2\hat{\Gamma}_p(1-\chi)}{2\hat{\Gamma}_p(1-\chi) + \pi D_p \ell_p / \ell_0} \right] \right\} \quad (25)$$

We set  $\ell_p = \lambda$  and define the dimensionless diffusiophoretic mobility and the dimensionless diffusion layer scale as

$$\Gamma_p^* = -\frac{\hat{\Gamma}_p}{\lambda U}, \quad \ell_0^* = \frac{\ell_0}{\lambda} \sim 1/Pe_p. \quad (26)$$

Thus, we can write expression (26) in dimensionless form as

$$\alpha = \alpha_0 \left\{ 1 - \Gamma_p^*(1-\chi)Pe_s + \frac{2\Gamma_p^{*2}(1-\chi)^2Pe_sPe_p\ell_0^*}{\pi} \ln \left[ \frac{2\Gamma_p^*(1-\chi)Pe_p\ell_0^*}{2\Gamma_p^*(1-\chi)Pe_p\ell_0^* - \pi} \right] \right\}. \quad (27)$$

- 
- [1] Jotkar M. and Cueto-Felgueroso L. Particle separation through diverging nanochannels via diffusiophoresis and diffusioosmosis. *Phys. Rev. Applied*, 16:064067, 2021.
- [2] A. D. Bordoloi, D. Scheidweiler, M. Dentz, Bouabdellaoui M., Abbarchi M., and de Anna P. Structure induced laminar vortices control anomalous dispersion in porous media. *Nat. Commun.*, 13:3820, 2022.
- [3] COMSOL Inc. <http://www.comsol.com/products/multiphysics/>, 2020.
- [4] M Abramowitz and I. A. Stegun. *Handbook of Mathematical Functions*. Dover Publications, New York, 1972.